

An atom trap system for practical ^{81}Kr dating

X. Du^{a)}

Physics Division, Argonne National Laboratory, Argonne, Illinois 60439 and Physics Department, Northwestern University, Evanston, Illinois 60208

K. Bailey, Z.-T. Lu,^{b)} P. Mueller, and T. P. O'Connor

Physics Division, Argonne National Laboratory, Argonne, Illinois 60439

L. Young

Chemistry Division, Argonne National Laboratory, Argonne, Illinois 60439

(Received 27 February 2004; accepted 6 July 2004; published 20 September 2004)

^{81}Kr ($t_{1/2}=2.3 \times 10^5$ yr, $^{81}\text{Kr}/\text{Kr} \sim 6 \times 10^{-13}$) is a long-lived cosmogenic isotope, which is ideal for dating old groundwater and ice in the age range of 50,000 years to 1 million years. Here, we describe the apparatus and performance of an atom-counting system for practical ^{81}Kr dating. This system is based upon the atom trap trace analysis method that was first demonstrated in 1999. Since then, significant improvements have been made to increase the system efficiency and to reduce the required krypton sample size. For a modern krypton gas sample of 100 μl STP, which contains 1.2×10^6 ^{81}Kr atoms, the system can accumulate approximately 240 ^{81}Kr counts in 20 h, thereby reaching a counting efficiency of 2×10^{-4} . Detailed studies have been conducted to characterize the performance of this system. This system has been calibrated with a low-level counting method and has been used for ^{81}Kr dating of ancient groundwater from the Nubian Aquifer (Egypt). It can also be used to measure the isotopic abundance of a fission-produced isotope ^{85}Kr ($t_{1/2} = 10.76$ year, $^{85}\text{Kr}/\text{Kr} \sim 2 \times 10^{-11}$). © 2004 American Institute of Physics.

[DOI: 10.1063/1.1790562]

I. INTRODUCTION

Much can be learned from the analysis of the ubiquitous long-lived radioactive isotopes. In the late 1940's, Libby and co-workers¹ first detected the cosmogenic isotope ^{14}C (5.7×10^3 yr, $^{14}\text{C}/\text{C} \sim 1 \times 10^{-12}$) in nature, and demonstrated that the analysis of ^{14}C could be used for archaeological dating. Since then, two well-established methods, low-level counting (LLC) and accelerator mass spectrometry (AMS), have been used to analyze ^{14}C and many other radioisotopes and to extract valuable information, regarding the production, transport, and decay processes of these isotopes. In groundwater research, ^{14}C dating is used to determine the sources, sinks, and flow patterns of large underground aquifers. In paleoclimate research, ^{14}C dating is used to determine the age of polar ice, which provides valuable information about the history of the Earth's climate. However, ^{14}C dating stops being effective as the ages of samples exceed approximately 50,000 years, or 9 half-lives of ^{14}C . In order to date older samples, a longer-lived radioisotope has to be employed. For this reason, ^{81}Kr ($t_{1/2}=2.3 \times 10^5$ yr) has been proposed as the ideal tracer isotope for dating old water and ice in the age range from 50,000 years to 1 million years.² ^{81}Kr is mainly produced in the upper atmosphere by cosmic-ray-induced spallation and neutron activation of stable krypton isotopes.² As a noble gas, ^{81}Kr is well mixed in the

Earth's atmosphere and possesses a homogeneous atmospheric isotopic abundance. Human activities involving nuclear fission have a negligible effect on the ^{81}Kr concentration because the stable ^{81}Br shields ^{81}Kr from the decay of fission products.³ These characteristics are essential for the reliable dating of geological samples and make ^{81}Kr the preferred isotope over several other cosmogenic isotopes of comparable half-lives, such as ^{10}Be and ^{36}Cl . Presently, any work on ^{81}Kr analysis is likely to encounter another radioactive krypton isotope, ^{85}Kr , which is a fission product of Uranium-235 and Plutonium-239, and is released into the atmosphere primarily by nuclear-fuel reprocessing plants. As a result, its abundance has increased by six orders of magnitude since the 1950's. ^{85}Kr can be used as a tracer to study air and ocean currents, date shallow groundwater, and monitor nuclear-fuel processing activities.

While the aforementioned applications are both important and attractive, the task of analyzing ^{81}Kr at or below the atmospheric level ($^{81}\text{Kr}/\text{Kr} \sim 6 \times 10^{-13}$) has always been an experimental challenge. LLC identifies radioactive isotopes by detecting their nuclear decays. LLC is often carried out in a specially designed underground laboratory in order to avoid background due to cosmic rays and the radioactivity present in common construction materials. LLC was first used to detect atmospheric ^{81}Kr and measure its abundance.⁴ For practical use, however, this method was inefficient and required a large amount (~ 1 liter STP) of Kr gas. The overwhelming decay events due to contamination by ^{85}Kr further render the method impractical. In general, counting atoms is a much better approach than counting decays in the analysis

^{a)}Current address: Department of Physics, University of Texas at Austin, Austin, TX 78712; electronic mail: du@physics.utexas.edu

^{b)}Electronic mail: lu@anl.gov

of long-lived isotope, such as ^{81}Kr . One such atom-counting method, resonance ionization mass spectrometry (RIMS), was also used to detect ^{81}Kr ,⁵ but only after the isotope was enriched to the level of $\sim 10^{-3}$ using several enrichment steps with different apparatus. Although, in principle, the efficiency of each step could be calibrated, and indeed the overall counting efficiency ($>50\%$) was impressive, the measurement procedure was rather complicated and only proof-of-principle measurements were performed. Variations of the RIMS method that do not require pre-enrichment are under development. The advantages of atom counting have indeed been realized with AMS, which has replaced LLC as the standard method of ^{14}C dating. Since krypton atoms do not form negative ions, ^{81}Kr cannot be analyzed at the standard AMS facilities that employ tandem accelerators. Recent work has shown that, by using an electron cyclotron resonance source to produce positive krypton ions and by using a higher energy (~ 4 GeV) accelerator to separate isobars, ^{81}Kr can be analyzed with AMS. Using the Michigan State University Superconducting Cyclotron, Collon *et al.*⁶ realized ^{81}Kr dating and determined the ages of groundwater, ranging from 200 to 400 kyr, at several sites in the Great Artesian Basin in Australia. With a detection efficiency of $\sim 1 \times 10^{-5}$, a 10% statistical precision measurement required a krypton gas sample of 0.5 cm^3 STP processed from 16 tons of groundwater. Improvements that would allow the use of a smaller and more accessible accelerator and that would result in a higher counting efficiency are under investigation.

Atom trap trace analysis (ATTA) is a relatively new atom-counting method first demonstrated in 1999, and was used to detect both ^{81}Kr and ^{85}Kr in natural atmospheric samples.⁷ It uses a table-top apparatus in a standard laboratory environment. In this method, an atom of a particular isotope is selectively captured by a magneto-optical trap (MOT)⁸ and then detected by observing its fluorescence. MOT is a type of robust and efficient atom trap, and consists of three orthogonal pairs of circularly polarized counter-propagating laser beams and a quadrupole magnetic field. Atoms can be trapped in a submillimeter size region for many seconds. The MOT is used here as a selective concentrator. When the laser frequency is tuned to within a few natural linewidths below resonance of the isotope of interest, only atoms of this particular isotope are trapped. Atoms of other isotopes are either deflected before reaching the trap or are allowed to pass through the trap without being captured. The detection method takes full advantage of the high selectivity of photon-burst spectroscopy.⁹ Detecting a single atom by observing its fluorescence induced with resonant laser excitation is, in general, difficult because of the low efficiency in photon collection ($\sim 10\%$) and photon counting ($\sim 10\%$), and the high background due to either scattered light or dark counts of the detector. These difficulties can be overcome by inducing from each trapped atom not only one, but 100 or even more photons in a short burst. The selectivity increases exponentially with the number of photons detected in a single burst as the overall selectivity (S) of a cycling excitation process is simply the product of the selectivity (s) of each excitation step, $S = s^n$, here n is the number of excitations. In ATTA, an atom can be trapped and

observed for 100 ms or longer, during which 10^6 fluorescence photons can be induced from a single trapped atom, and as many as 10^4 photons can be detected. Furthermore, the viewing region where the atoms are trapped and from which the fluorescence is collected is small (<1 mm across). Therefore, spatial filtering can easily be implemented to reduce the background photons scattered off the windows and walls of the vacuum chamber. These advantages allow the counting of single atoms to be implemented with a high signal-to-noise ratio as well as a superb selectivity. Indeed ATTA is immune to interference from other isotopes, elements, or molecules. The selectivity of ATTA is only statistically limited by the atomic beam flux, or, more specifically, by the number of atoms that can be sent through the trap in a practical time period.

The system as reported in 1999 had a counting efficiency of $\sim 1 \times 10^{-7}$. Use of that system to measure the abundance of ^{85}Kr with a statistical precision of 10% requires a krypton sample of 3 cm^3 STP, while measurement of ^{81}Kr to 10% requires a krypton sample of 60 cm^3 STP. This limited the system to atmospheric applications where large samples are available. Since then, system improvements including a more intense source of metastable Kr atoms, a recirculating vacuum system, and better optical arrangements have been made. At present, the system efficiency has reached 2×10^{-4} and the counting rate has increased by a factor of 3. The required krypton sample size has been reduced to below $100 \mu\text{l}$ STP of Kr. The improved ATTA system has been calibrated with LLC to demonstrate its capability on quantitative measurements.¹⁰ Recently, the system has been used to measure the $^{81}\text{Kr}/\text{Kr}$ ratios in deep groundwater from the Nubian Aquifer and the ages of the groundwater (ranging from 200 kyr to 1000 kyr) are derived from the ratio measurements.¹¹

In this article, we describe in detail the apparatus and the performance of the new system. The relevant atomic transitions of krypton are introduced in Sec. II. The system apparatus, including the lasers and optics, and the vacuum system, is described in Sec. III. The ^{85}Kr , ^{81}Kr abundance measurements, and systematic analysis are presented in Sec. IV. The future outlook is provided in Sec. V.

II. RELEVANT ATOMIC TRANSITIONS

Figure 1 shows the atomic level diagram of krypton. The excitation of the first allowed transition from the ground-level $4p^6(^1S_0)$ to an intermediate level $5s[3/2]_1$, requires vacuum ultraviolet (VUV) photons at a wavelength of 124 nm. A MOT based on this transition is impossible with present laser technology as continuous-wave lasers of this wavelength are far from having sufficient power needed for trapping. On the other hand, Kr atoms can be excited from the ground level to a metastable level $5s[3/2]_2$ (lifetime ~ 40 s) via electron-impact or photon excitations. Laser trapping and cooling of Kr^* (metastable Kr) based on the transition $5s[3/2]_2 \rightarrow 5p[5/2]_3$ have been realized with the laser of 811 nm wavelength. Note that the selection rules that slow down the decay of Kr^* atoms break down easily upon collisions of the Kr^* atoms with the ground-level Kr atoms, other

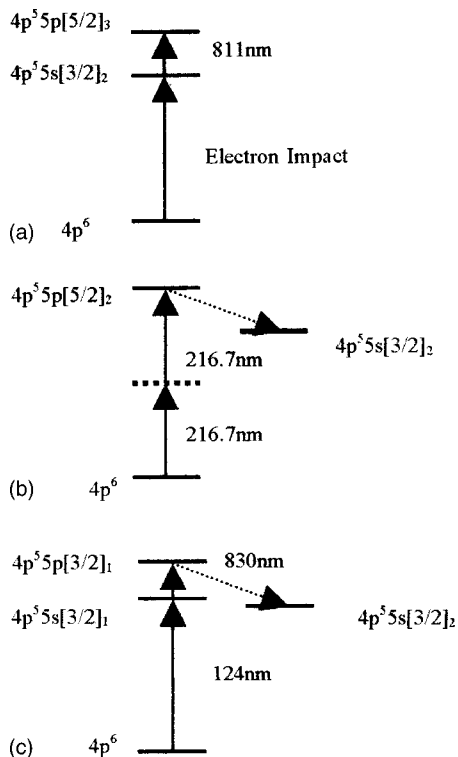


FIG. 1. Krypton energy level diagrams. (a) Excitation scheme used in the laser trapping of Kr^* atoms. (b) Populating the metastable level via a non-resonant UV+UV excitation. (c) Populating the metastable level via a resonant VUV+IR excitation.

atoms, molecules, or surfaces. This characteristic makes Kr^* fragile and difficult to produce. On the other hand, the lack of a background of Kr^* makes individual trapped atoms easier to detect.

For even Kr isotopes, the transition $5s[3/2]_2 \rightarrow 5p[5/2]_3$ is “closed”, i.e., the excited atoms will decay back to the lower states from where it will be re-excited by the laser light. For odd isotopes (^{83}Kr , ^{85}Kr , and ^{81}Kr), the metastable level $5s[3/2]_2$ and the upper level $5p[5/2]_3$ split into numerous energy levels due to hyperfine interaction. The hyperfine structures of the odd isotopes are shown in Fig. 2. For ^{83}Kr and ^{85}Kr , we use the transition $F=13/2 \rightarrow F'=15/2$ to cool and trap the atoms (for ^{81}Kr , we use $F=11/2 \rightarrow F'=13/2$). In practice, those transitions are not perfectly closed. It is possible that, for ^{83}Kr and ^{85}Kr , the atoms will be excited to the neighboring upper states $F'=13/2$ or $F'=11/2$ (for ^{81}Kr , $F'=11/2$ or $F'=9/2$) and then decay back to $F=11/2$ or $F=9/2$ (for ^{81}Kr , $F=9/2$ or $F=7/2$) so that the atoms will no longer interact with the laser light tuned to the resonance of $F=13/2 \rightarrow F'=15/2$ (for ^{81}Kr , $F=11/2 \rightarrow F'=13/2$). Those atoms will become “dark” to the laser light. This can happen every few hundred cycles when the laser frequency is tuned to the trapping transition and the intensity of laser beam is 10 mW/cm^2 (the saturation intensity is 2.6 mW/cm^2). To pump the atoms out of those dark lower levels, laser light with “sideband” frequencies (for ^{83}Kr and ^{85}Kr , $F=11/2 \rightarrow F'=13/2$ and $F=9/2 \rightarrow F'=11/2$; for ^{81}Kr , $F=9/2 \rightarrow F'=11/2$ and $F=7/2 \rightarrow F'=9/2$) is needed. Moreover, the sidebands are essential to trap the odd isotopes of krypton at a high capture rate and to increase the lifetime of single atoms in the trap.

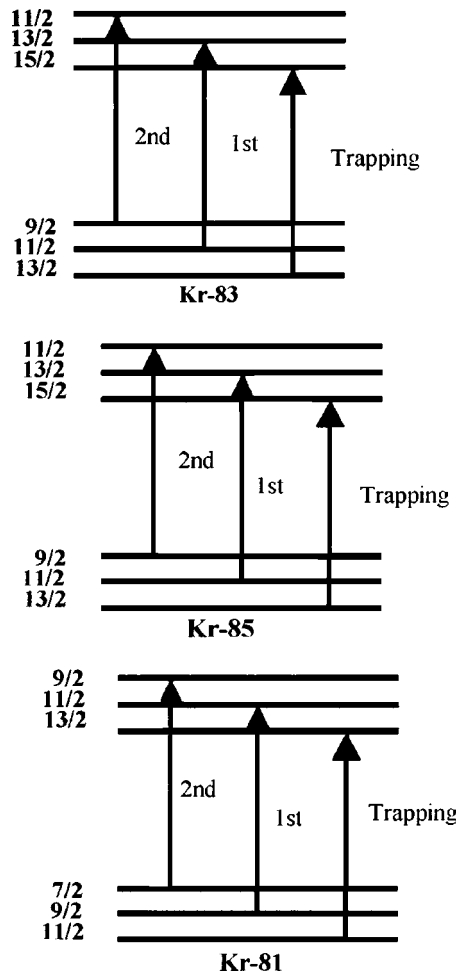


FIG. 2. Hyperfine structures of the odd krypton isotopes. Note only the levels relevant to trapping are drawn.

Atoms of different isotopes have different isotopic shifts due to their variations in the nuclear mass, volume, and moments. When the laser frequency is tuned to the resonance of the isotope of interest, only atoms of that particular isotope are trapped. Figure 3 shows the fluorescence signals of trapped Kr^* atoms when the laser frequency is scanned through the resonance of different krypton isotopes. The resonance frequency positions of rare isotopes are also marked in the figure.

III. SYSTEM APPARATUS

We employ an all-diode-laser system in this apparatus as shown in Fig. 4. A low-power external cavity diode laser (SDL-5401, 12 mW output) serves as the master laser and is used to injection lock two high-power diode lasers (SDL-5422, 100 mW output) and one tapered amplifier (Toptica TA-0810, 500 mW output), which supply the laser beams for transverse cooling, slowing, and trapping of Kr^* atoms. The frequency of the master laser, after an approximately 800 MHz offset generated by a tunable acousto-optic modulator [(AOM) Brimrose, TEF-380-200] to compensate for isotope shifts, is locked to the resonance of the $5s[3/2]_2 \rightarrow 5p[5/2]_3$ transition of ^{84}Kr in a reference vapor cell. The two sidebands are generated by sending the laser beam through a tunable traveling-wave electro-optic modulator

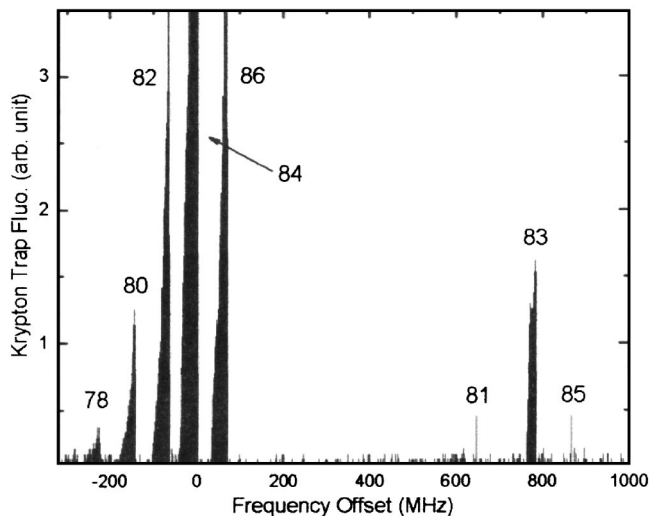


FIG. 3. Fluorescence of trapped Kr* atoms. Dark bands are the signal of stable isotopes measured with a *p-i-n* photodiode detector. Line markers mark the frequency positions of the two rare isotopes.

[(EOM) Quantum Technology, TWAP-11]. The electronic tuning of the AOM frequency and the electronic tuning of the two EOM frequencies allow us to tune the laser frequencies to match the transitions (trapping and repumping) of ⁸³Kr, ⁸⁵Kr, and ⁸¹Kr, respectively. In order to avoid the possibility of exciting any unintended transitions inside the Zeeman

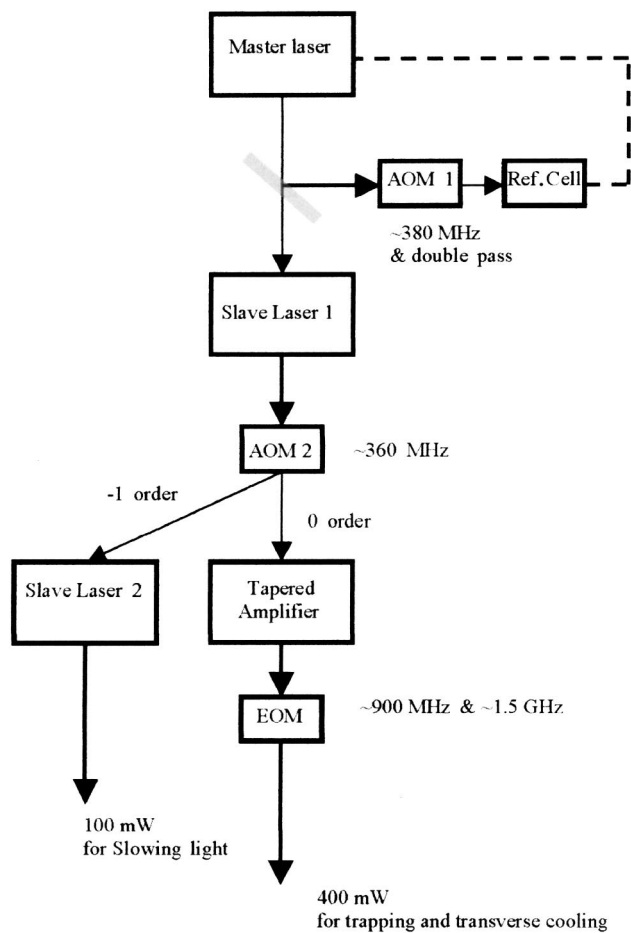


FIG. 4. Diagram of laser setup.

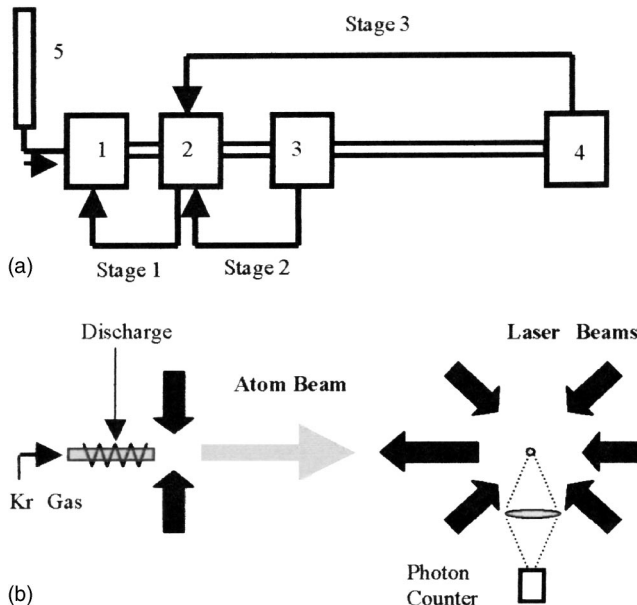


FIG. 5. (a) Diagram of the vacuum system. In the measurement: 1. Source chamber—4 mTorr (with 100 l/s getter pump); 2. Transverse cooling chamber— 2×10^{-5} Torr (with 270 l/s turbopump); 3. Chopper chamber— 2×10^{-7} Torr (with 150 l/s turbopump); 4. Trap chamber— 6×10^{-8} Torr (with 200 l/s turbopump); and 5. Reservoir—150 mTorr after filling 100 μ L STP of krypton sample. (b) Schematic of the experimental setup.

man slower, where the hyperfine structure is further complicated due to Zeeman shifts, the sidebands are added to the laser beams of transverse cooling and trapping only, not to the slowing laser beam.

The vacuum system, shown in Fig. 5(a), consists of the following components: The sample reservoir, the source chamber, the transverse cooling chamber, the chopper chamber, and the trap chamber. The system is differentially pumped by three turbopumps to maintain a pressure of a few mTorr in the source chamber and a pressure of $\sim 10^{-8}$ Torr in the trap chamber. A getter pump (SAES, GP50) in the source chamber removes the reactive gases, such as hydrogen, water, etc., from the vacuum system while leaving the noble gases, including the Kr sample, intact. A novel feature of the system is that it can be switched into a mode which repeatedly circulates the Kr atoms through the vacuum system and significantly improves the counting efficiency. Ideally, the Kr sample can be indefinitely recirculated inside the vacuum system, however, the recirculation time is limited by two factors: Cross-sample contamination (discussed in Sec. IV D) and argon (Ar) outgassing. Argon, as a part of the outgassing of the vacuum system, accumulates in the recirculation mode. Over 10 h, the partial pressure of Ar can increase from below 10^{-9} Torr to 1×10^{-7} Torr, or 50% of the Kr partial pressure (in the chopper chamber). As a result, the Kr* beam flux is reduced as is the counting rate of ⁸¹Kr. This effect requires the system to be pumped out after 10 h of recirculation and to be then refilled. The loss of Kr sample during the pump-out limits the average recirculation cycles to approximately 2000, and the counting efficiency of the system to 2×10^{-4} .

For an analysis, the Kr sample is first transferred from a steel sample container to the reservoir. The reservoir has a

volume of 0.47 L, and a Baratron pressure gauge (1 Torr maximum) is used to measure the initial amount of gas sample as well as the gas consumption rate during the measurement. The maximum amount of gas sample that can be measured in the reservoir is 500 μL STP. The Kr sample is injected from the reservoir through a fine leak valve into the source chamber where a rf-driven discharge is used to produce the Kr^* atoms. The rf-discharge source design has been described in detail in our previous paper.¹² Kr gas flows from the source chamber into the transverse cooling chamber through a 18 cm long and 1 cm diameter glass tube, in which a plasma is produced by rf power coupled through a surrounding coil. In this plasma region, atoms are excited into the metastable level $5s[3/2]_2$ via collisions with energetic electrons and ions. Laser spectroscopy techniques are used to measure the beam flux and the velocity distribution of the Kr^* beam. The Kr^* beam flux is optimized when the pressure is approximately 4 mTorr in the source chamber and 2×10^{-5} Torr in the transverse cooling chamber. Under these conditions, the Kr^* beam has an angular flux density of $4 \times 10^{14} \text{ s}^{-1} \text{ sr}^{-1}$, a Kr^*/Kr ratio of 1×10^{-3} in the forward direction, and the most probable velocity of 300 m/s. In the transverse cooling chamber, the Kr^* beam is cooled in both transverse directions by two sets of laser beams, each of which has an intensity of $\sim 35 \text{ mW/cm}^2$ and is multiply reflected over a length of 10 cm along the atomic beam between two flat mirrors. The Kr^* trap loading rate is increased by a factor of 20 with two-dimensional transverse cooling. Note that this transverse-cooling process is isotopically selective; it only enhances the forward Kr^* beam flux of the selected isotope. The chopper chamber houses a rotating mechanical chopper that periodically blocks the Kr^* beam, essentially turning on and off the beam going into the trap chamber. The chopper chamber also houses a residual gas analyzer (SRS, RGA200) for monitoring the partial pressures of different gases in the vacuum system. Downstream from the chopper chamber, the Kr^* atoms enter a 1.2 m long Zeeman slower, where they are decelerated by a 30 mW circularly polarized laser beam from a velocity of approximately 300 m/s near the source down to 20 m/s as they enter the trap chamber.

In the trap chamber, a MOT is used to capture the slow Kr^* atoms and confine them in a submillimeter region in the center of the chamber. The MOT toggles between two modes (shown in Fig. 6). One mode is optimized for maximum capture rate, and the other for single atom detection. In the capture mode, each of the six laser trapping beams has a diameter of 3 cm and an intensity of 10 mW/cm^2 , and the quadrupole magnetic field has a field gradient of 3 Gauss/cm. The large and intense laser beams, along with the small field gradient, increase the volume where atoms are captured. Under the optimum conditions, the capture rate of ^{83}Kr reaches $1 \times 10^9 \text{ s}^{-1}$. Assuming equal capture efficiencies for the rare isotopes, we expect a capture rate of approximately 20 atoms per hour for ^{81}Kr and 720 atoms per hour for ^{85}Kr from a modern atmospheric sample. Since the pressure of the trap chamber is 6×10^{-8} Torr and the lifetime of the trapped Kr^* atoms is approximately 0.5 s, the rare Kr^*

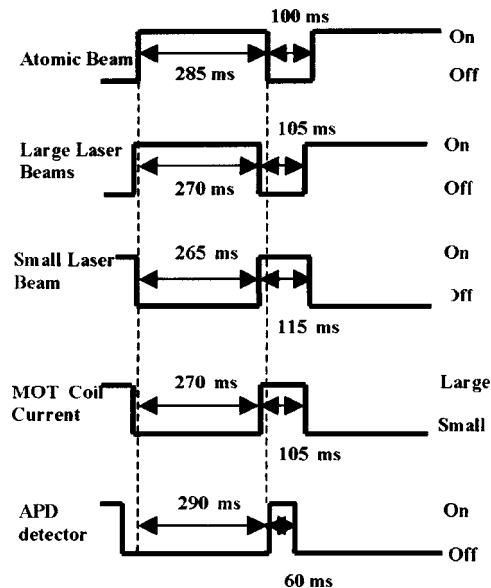


FIG. 6. Timing diagram for single atom counting.

atoms cannot be accumulated in the trap. Instead, they are usually captured and counted by one at a time.

For single atom detection, the main technical challenge is to reduce the background photons scattered off walls, windows, and even the optics outside the vacuum chamber. It takes at least 10 mW of laser light to maintain the trap, compared with only approximately 1 pW of light emitted by a trapped atom. In the detection mode, in order to reduce scattered light, the diameter and intensity of trapping beams are reduced to 1 cm and 2 mW/cm^2 , respectively. The switching is implemented without interruption of trapping laser beams so that the trapped atom does not escape during the switching. Meanwhile, in order to squeeze the trapped atom into a smaller volume and increase its image brightness, the magnetic field gradient is increased to 10 Gauss/cm. Moreover, the inner surface of the trap chamber is covered by vacuum-compatible black paint (AZ Technology, MLS-85SB), and all of the nearby mirrors and quarter-wave plates are carefully aligned, and sometimes deliberately misaligned, to achieve a low level of background light. A single trapped Kr^* atom scatters photons at a rate of $\sim 10^7 \text{ s}^{-1}$, 1% of which is collected and imaged by a pair of numerical aperture = 0.5 lenses, through a 0.5 mm diameter aperture which spatially filters out most of the diffuse background light, and reimaged by another pair of lenses onto a 0.6 mm diameter avalanche photodiode with a photon counting efficiency of 25% at 811 nm wavelength. The resulting single atom signal is 13 kHz photon counts and the background is 13 kHz [Fig. 7(a)]. In a 60 ms counting period, the single atom detection achieves a signal-to-noise ratio of 30.

IV. ^{81}Kr AND ^{85}Kr ABUNDANCE MEASUREMENTS

A. Control isotope and ratio measurements

In ^{81}Kr dating, age is defined as the period since the time when samples of water and ice were near surface and had contact with the atmosphere. Once the water went under-

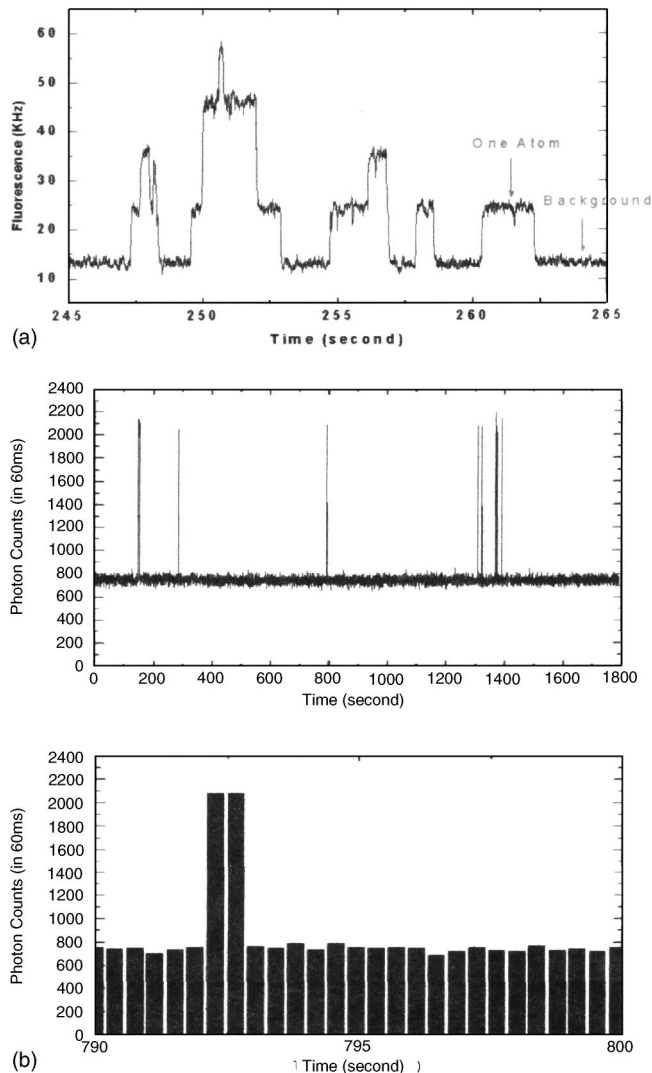


FIG. 7. Single atom detection: (a) A time slot of signal of ⁸³Kr at the level of single atoms and (b) Signal of a single ⁸¹Kr atom. During loading time, the photon-count rate is low because the counter is blocked for protection from overexposure.

ground and ice froze, they were separated from the atmosphere, and the ⁸¹Kr abundance started to decay following

$$N(t) = N_0 e^{-t/\tau} \tag{1}$$

Here, τ is the lifetime of ⁸¹Kr, N_0 is the modern atmospheric isotopic abundance of ⁸¹Kr (⁸¹Kr/Kr), $N(t)$ is the isotopic abundance of ⁸¹Kr in the sample, and t is the age of the sample.

The capture rate of an individual isotope depends on many parameters of the apparatus including the rf-discharge intensity, gas flow rate, various vacuum pressures, partial pressure of Kr, laser power, laser frequencies, laser beam alignment, etc. Our system is stable after 0.5 h of warm up. The capture rate of ⁸³Kr typically drifts by less than 15% in a 10 h run. For the analysis, the capture rates of both ⁸¹Kr and a control isotope, ⁸³Kr or ⁸⁵Kr, are measured, and the ⁸¹Kr abundance is determined by the ratio of the two capture rates. By frequently switching the system between counting ⁸¹Kr and counting the control isotope, much of the common-mode noise due to the variation of all the parameters is can-

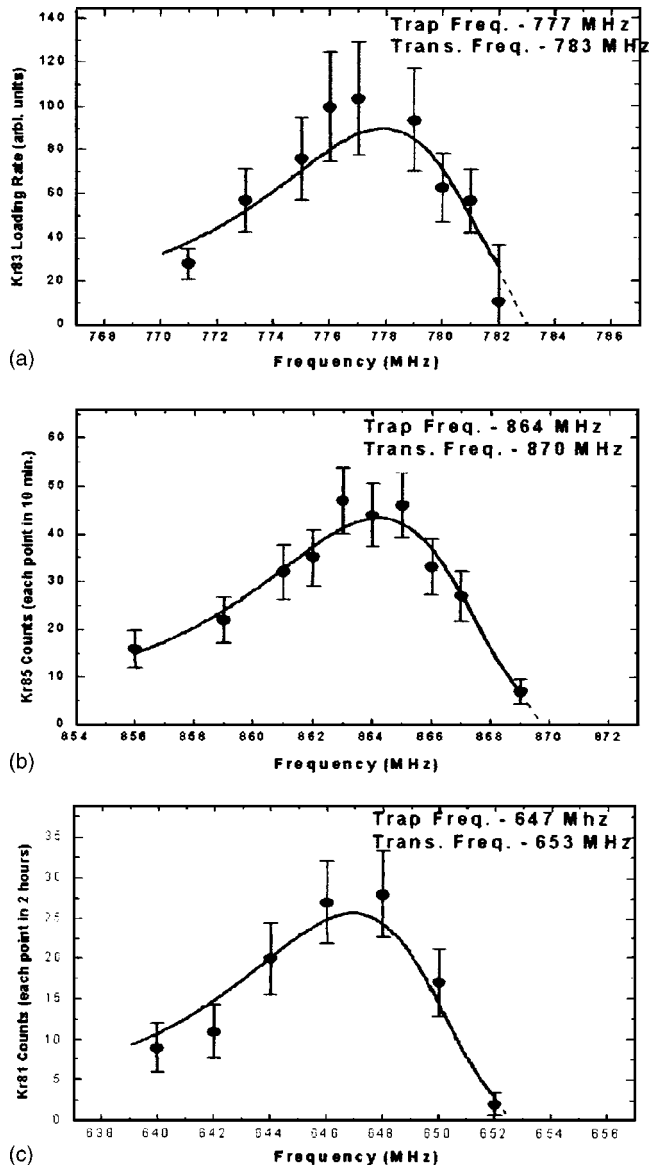


FIG. 8. The dependence of capture rates on laser frequencies. (a) ⁸³Kr capture rate vs trapping light frequency. (b) ⁸³Kr capture rate vs trapping light frequency. (c) ⁸¹Kr capture rate vs trapping frequency.

celled out in the ratio. Furthermore, the age is determined by the ratio of the ⁸¹Kr abundance in the sample and in the atmosphere; it is in fact a ratio of ratios, which further reduces the systematic effects.

In principle, the stable ⁸³Kr can be used as the control isotope. In practice, however, its capture rate of $\sim 10^9$ s⁻¹ is so much higher than the capture rate of ⁸¹Kr that, instead of single atom counting, it requires a low-gain photodetector to measure the fluorescence of the trapped ⁸³Kr atoms. Moreover, due to collisions between trapped atoms, the lifetime of trapped ⁸³Kr atoms (~ 10 ms) is much smaller than that of a single trapped ⁸¹Kr atom (~ 0.5 s). The large differences in trap parameters make ⁸³Kr a less reliable control isotope. On the other hand, ⁸⁵Kr at the isotopic abundance level of 10^{-11} can be introduced into the sample and calibrated accurately with the LLC method. The “spiked” ⁸⁵Kr can then be counted at the single atom level and serve as a reliable control isotope. The age of the sample can be calculated as

TABLE I. Trapping transition frequencies and sideband frequencies for ^{83}Kr , ^{85}Kr , and ^{81}Kr .

		Cannon's work (Ref. 13)	Our work
^{83}Kr	Trapping transition	786.9 MHz	783 MHz
	First sideband	-88.9 MHz	-87 MHz
	Second sideband	-711.8 MHz	-707 MHz
^{85}Kr	Trapping transition	868.7 MHz	870 MHz
	First sideband	-76.4 MHz	-78 MHz
	Second sideband	-687.2 MHz	-676 MHz
^{81}Kr	Trapping transition	651.8 MHz	653 MHz
	First sideband	-308.5 MHz	
	Second sideband	-795.9 MHz	

$$t = \tau \ln \left[\frac{N_{81a}/(N_{85a}\rho_{85s})}{N_{81s}/(N_{85s}\rho_{85a})} \right]. \quad (2)$$

Here, N_{81s} and N_{81a} are counts of ^{81}Kr atoms from the sample and from air, respectively; N_{85s} and N_{85a} are counts of ^{85}Kr atoms from the sample and air, respectively; ρ_{85s} and ρ_{85a} are the LLC measurement of the $^{85}\text{Kr}/\text{Kr}$ in the sample and air, respectively. The spike and LLC of ^{85}Kr involve mature technologies, and are practiced on a routine basis in a few selected labs around the world.

B. Procedure

For an analysis, the system is filled to the operation condition with 30 μl STP of Kr sample, which lasts for 10 h before the accumulation of Ar requires the system to be pumped out and refilled. An analysis run consists of many cycles, with each cycle lasting approximately 40 minutes: 10 min for counting ^{85}Kr followed by 30 min for counting ^{81}Kr . From measuring one isotope to the other, there are only three parameters to switch: Isotope shift which is controlled by the AOM frequency and the two sidebands which are controlled by the EOM frequencies. The switching is performed either manually or automatically with computer control.

Detailed $^{85}\text{Kr}/^{81}\text{Kr}$ measurement results can be found in our recent paper.¹⁰

C. Systematic: Frequency dependence

Laser frequency setting affects the capture rates. It affects the abundance measurement, which is done by measuring the ratio of capture rates of two different isotopes, but it should not affect the age, which is derived from the abundances of two samples (the ratio of ratios) ideally analyzed under identical laser frequency setting. Therefore, the repeatability of the laser frequency setting from one analysis to another is crucial to age determination. A drift in laser frequencies can cause a systematic error in age. This effect is

studied by mapping out the dependence of capture rates of ^{83}Kr , ^{85}Kr , and ^{81}Kr on various laser frequencies. Furthermore, in order to count the atoms at the maximum capture rate, we also need to find out the optimum frequency settings.

From Fig. 8(a), we conclude that the optimum trapping frequency for ^{83}Kr is 6 MHz redshifted from its trapping transition. For ^{85}Kr [Fig. 8(b)], the maximum capture rate is approximately 45 atoms/10 min and a 10 min measurement is performed at each frequency point. The optimum trapping frequency is approximately 864 MHz blueshifted to the ^{84}Kr atomic transition. Assuming that the optimum trapping frequency for ^{85}Kr is 6 MHz redtuned to its transition, we can derive that its trapping transition frequency is 870 MHz blueshifted to the ^{84}Kr transition. For ^{81}Kr [Fig. 8(c)], the maximum capture rate is approximately 14 atoms/h and 2 h measurement is performed at each point. The optimum trapping frequency is 647 MHz. Its trapping transition frequency is 653 MHz blueshifted to the ^{84}Kr transition if we use the same assumption as for ^{83}Kr and ^{85}Kr . Our trapping transition frequency results are in good agreement with the results in Cannon's paper.¹³ The laser frequency, locked to the $5s[3/2]_2 \rightarrow 5p[5/2]_3$ transition of ^{84}Kr in the vapor cell, has a repeatability of better than 0.5 MHz, which should cause the capture rate to shift by less than 4%.

We have also mapped out the capture rate versus the first sideband frequency, and the capture rate versus the second sideband frequency for both ^{83}Kr and ^{85}Kr . The results (listed in Table I) are in good agreement with Cannon's work.¹³ For either isotope, the capture rate drops by a factor of 2 when the first sideband frequency is tuned 20 MHz away from its optimum frequency setting and drops by a factor of 2 when the second sideband is 40 MHz away from the optimum frequency setting. This insensitive frequency dependence is due to power broadening: the rates of repumping transition provided by the laser intensity of the sidebands far exceed the needed repumping transition rates. We conclude that the ef-

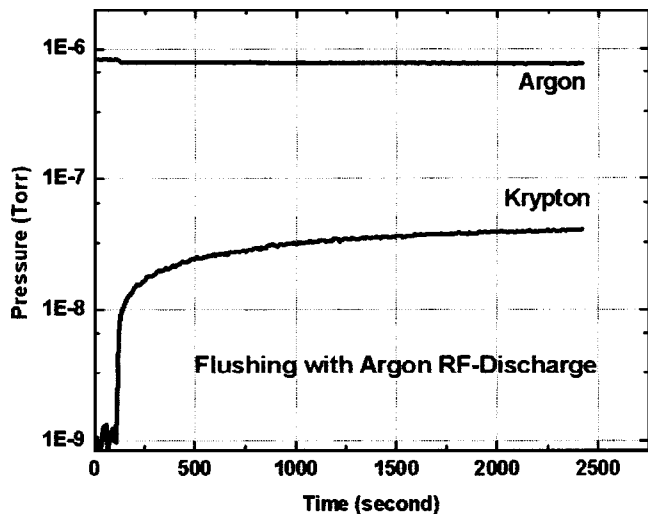


FIG. 9. Test of cross-sample contamination.

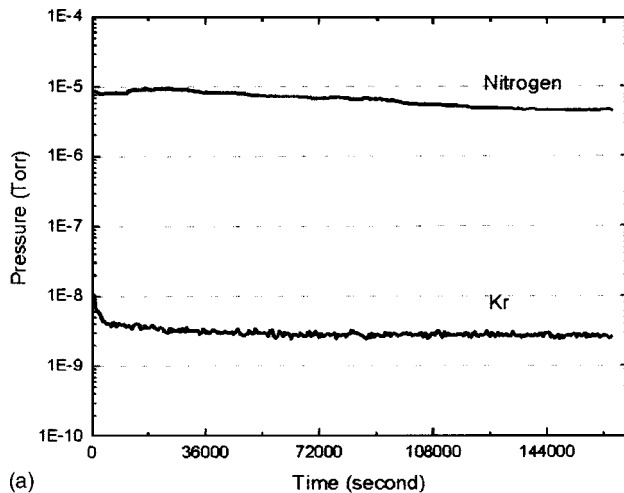
fect on capture rates due to any changes of sidebands is negligible.

D. Systematic: Cross-sample contamination

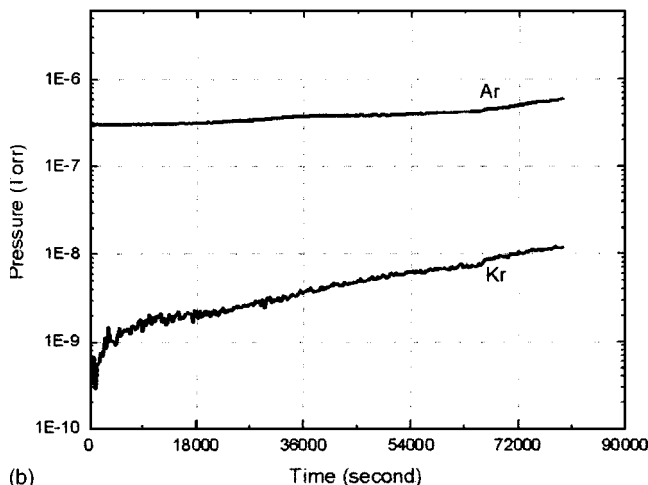
When the rf discharge is on, a small fraction of the Kr atoms are ionized, accelerated by the rf electromagnetic field, and imbedded into the glass tube surface. At the same time, the embedded Kr atoms are released into the vacuum chamber by the discharge. We observed an initial reduction of 3 μl STP of Kr, or 10% of the sample size in one fill, during 2 h after turn-on of the discharge; and a total reduction of 6 μl STP, or 20% of one fill, in 8 h. The loss rate gradually decreases to zero as the Kr atoms in the vacuum chamber reach equilibrium with the embedded Kr atoms. We maintain a constant Kr partial pressure by refilling up to 5% of one-fill Kr gas for a few times throughout the experiment. Obviously, the embedded Kr atoms would be a serious source of cross-sample contamination. This is confirmed in the following test. After one measurement, the vacuum system is pumped out and then filled with Ar. The partial krypton pressure dramatically increases when the Ar discharge is on, shown in Fig. 9. The amount of Kr released is measured to be 3 μl STP in 0.5 h.

The cross-sample contamination effect is mitigated by flushing the system with the discharge of nitrogen (N₂) or Ar. We prefer using N₂ because it can be removed by the getter pump. The result is shown in Fig. 10. The system is flushed with N₂ discharge for more than 45 h. Then, the system is filled with Ar and the Ar discharge is turned on. In 10 h the partial krypton pressure increases up to 4 × 10⁻⁹ Torr, or 2% of one-fill krypton sample; in 20 h, the krypton pressure increases up to 1 × 10⁻⁸ Torr, or 5% of one-fill krypton sample. Note that the average contamination in a run is one-half of the final contamination level. In the experiment,^{10,11} the system is flushed for 14 h between samples. The average amount of residual krypton present during a 10 h measurement is (4 ± 2)% of the Kr sample in the system.

The effect of contamination on age is expressed as follows:



(a)



(b)

FIG. 10. (a) Flushing the glass tube with nitrogen discharge. (b) Test of contamination after flushing.

$$t = \tau \ln \left(R \frac{1}{1 - (R - 1)\epsilon} \right), \tag{3}$$

where *t* is the age of the sample, τ is the lifetime of ⁸¹Kr, *R* is (⁸¹Kr/Kr)_{air} / (⁸¹Kr/Kr)_{sample}, the measured ratio of ratios of modern Kr and samples, and ϵ is the contamination level. Note that here we assume the contamination is only from modern Kr.

E. Error in measurements of the age of samples

The error in measurements of the age of samples is a combination of the error of ATTA measurements and the error of LLC measurements. The error of ATTA measurements is comprised of a statistical error of ⁸¹Kr counts (~100 in 10 h measurement for modern Kr samples), a 5% systematic error due to the uncertainties in laser frequency settings, and an error in the correction for the memory effect. For the Kr samples in the age range of 300 000 years or younger (*R* < 3), the error of ATTA measurements is dominated by the statistical error of ⁸¹Kr counts, while for the samples in the age range of 1 million years or older (*R* ~ 20), the error in the correction for the memory effect dominates and ultimately limits the maximum age (~1 million years) of

samples that ATTA can measure. The error of LLC measurements is dominated by the statistical error of ^{85}Kr counts ($<10\%$).

V. OUTLOOK

Whereas incremental improvements of both the efficiency and counting rate are possible with more laser power and by implementing more sophisticated transverse cooling scheme, a more dramatic improvement should be possible by replacing the rf-discharge Kr^* source with a photon-excitation method as illustrated in Figs. 1(b) and 1(c). In a recent study by Young *et al.*,¹⁴ Kr^* was produced by a two-photon excitation induced with a VUV lamp (124 nm) and a near-infrared laser (819 nm). This scheme promises to improve both the efficiency and counting rate by at least a factor of 20. It will also significantly reduce the cross-sample contamination effect.

ACKNOWLEDGMENTS

This work is supported by the U.S. Department of Energy, Nuclear Physics Division, and by the Office of Basic Energy Sciences, Division of Chemical Sciences, under Contract No. W-31-109-ENG-38.

- ¹J. R. Arnold and W. F. Libby, *Science* **110**, 678 (1949).
- ²H. Oeschger, *Nucl. Instrum. Methods Phys. Res. B* **29**, 196 (1987).
- ³P. Collon, T. Antaya, B. Davids, M. Fauerbach, R. Harkewicz, M. Hellstrom, W. Kutschera, D. Morrissey, R. Pardo, M. Paul, B. Sherrill, and M. Steiner, *Nucl. Instrum. Methods Phys. Res. B* **123**, 122 (1997).
- ⁴H. H. Loosli and H. Oeschger, *Earth Planet. Sci. Lett.* **7**, 67 (1969).
- ⁵N. Thonnard, R. D. Willis, M. C. Wright, W. A. Davis, and B. E. Lehmann, *Nucl. Instrum. Methods Phys. Res. B* **29**, 398 (1987).
- ⁶P. Collon, W. Kutschera, H. H. Loosli, B. E. Lehmann, R. Purtschert, A. Love, L. Sampson, D. Anthony, D. Cole, B. Davids, D. J. Morrissey, B. M. Sherrill, M. Steiner, R. C. Pardo, and M. Paul, *Earth Planet. Sci. Lett.* **182**, 103 (2000).
- ⁷C. Y. Chen, Y. M. Li, K. Bailey, T. P. O'Connor, L. Young, and Z.-T. Lu, *Science* **286**, 1139 (1999).
- ⁸E. L. Raab, M. Prentiss, A. Cable, S. Chu, and D. E. Pritchard, *Phys. Rev. Lett.* **59**, 2631 (1987).
- ⁹W. M. Fairbank Jr., *Nucl. Instrum. Methods Phys. Res. B* **29**, 407 (1987).
- ¹⁰X. Du, R. Purtschert, K. Bailey, B. E. Lehmann, R. Lorenzo, Z.-T. Lu, P. Mueller, T. P. O'Connor, N. C. Sturchio, and L. Young, *Geophys. Res. Lett.* **30**, 2068 (2003).
- ¹¹N. C. Sturchio, X. Du, R. Purtschert, B. E. Lehmann, M. Sultan, L. J. Patterson, Z.-T. Lu, P. Mueller, K. Bailey, T. P. O'Connor, L. Young, R. Lorenzo, B. M. Kennedy, M. van Soest, Z. El Alfy, B. El Kaliouby, Y. Dawood, and A. M. A. Abdallah, *Geophys. Res. Lett.* **31**, L05503 (2004).
- ¹²C. Y. Chen, K. Bailey, Y. M. Li, T. P. O'Connor, Z.-T. Lu, X. Du, L. Young, and G. Winkler, *Rev. Sci. Instrum.* **72**, 271 (2001).
- ¹³B. D. Cannon, *Phys. Rev. A* **47**, 1148 (1993).
- ¹⁴L. Young, D. Yang, and R.-W. Dunford, *J. Phys. B* **35**, 2985 (2002).